



Controlling the energetic characteristics of micro energy storage device by in situ deposition Al/MoO₃ nanolaminates with varying internal structure



Jianbing Xu^a, Yun Shen^a, Chengai Wang^a, Ji Dai^a, Yu Tai^a, Yinghua Ye^{a,*}, Ruiqi Shen^a, Haiyang Wang^b, Michael R. Zachariah^b

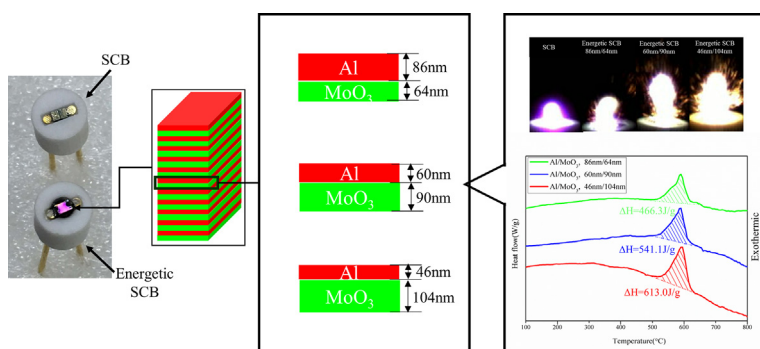
^a Department of Applied Chemistry, School of Chemical Engineering, Nanjing University of Science and Technology, Nanjing 210094, China

^b Department of Chemical and Environmental Engineering, University of California Riverside, Riverside, CA 92521, USA

HIGHLIGHTS

- In situ integrated Al/MoO₃ nanolaminates to fabricate micro energy storage device.
- These devices showed controllable energy release ability with tunable nanolaminates.
- Condensed state reaction mechanism was revealed in these nano multi-layered films.

GRAPHICAL ABSTRACT



ARTICLE INFO

Keywords:

Energy storage
In situ integration
Energetic nanolaminate
Al/MoO₃
Micro initiator

ABSTRACT

The control of energy storage and release in micro energy devices is important and challenging for utilization of energy. In this work, three kinds of micro energy storage devices were fabricated through in situ integrating different aluminum/molybdenum trioxide (Al/MoO₃) nanolaminates on a semiconductor bridge. The morphology and composition characterizations confirm that Al layer and MoO₃ layer closely contacted with different single thickness, endowing the Al/MoO₃ nanolaminates with variable heat release from 466.3 J/g to 613.0 J/g. Meanwhile, these devices demonstrate controllable energy release ability showing the flame durations of 60–600 μs (discharged with 47 μF/50 V) by simply changing the Al and MoO₃ accumulate structure in Al/MoO₃ nanolaminates. Preliminary reaction mechanism obtained by probing the reaction in argon and vacuum atmosphere suggests that condensed state reaction process was confirmed in these nano multilayered films. This result may yield significant advantages in developing a tailored architecture for micro ignition applications.

1. Introduction

The utilization of energy, which consists of energy storage and release, is one of the great challenges in the twenty-first century. Energy stored in a chemical compound is considered to be one of the most

important energy storage systems from ancient charcoal to recent oil, fossil [1–3]. This kind of energy storage materials are used as fuel which store solar energy and then release it with heat, light by breaking chemical bonds and reforming new molecular bonds in product accompanied with oxidation reaction [4]. Therefore, the structure and

* Corresponding author.

E-mail address: yyinghua@njust.edu.cn (Y. Ye).

<https://doi.org/10.1016/j.cej.2019.04.205>

Received 12 February 2019; Received in revised form 8 April 2019; Accepted 28 April 2019

Available online 30 April 2019

1385-8947/ © 2019 Elsevier B.V. All rights reserved.

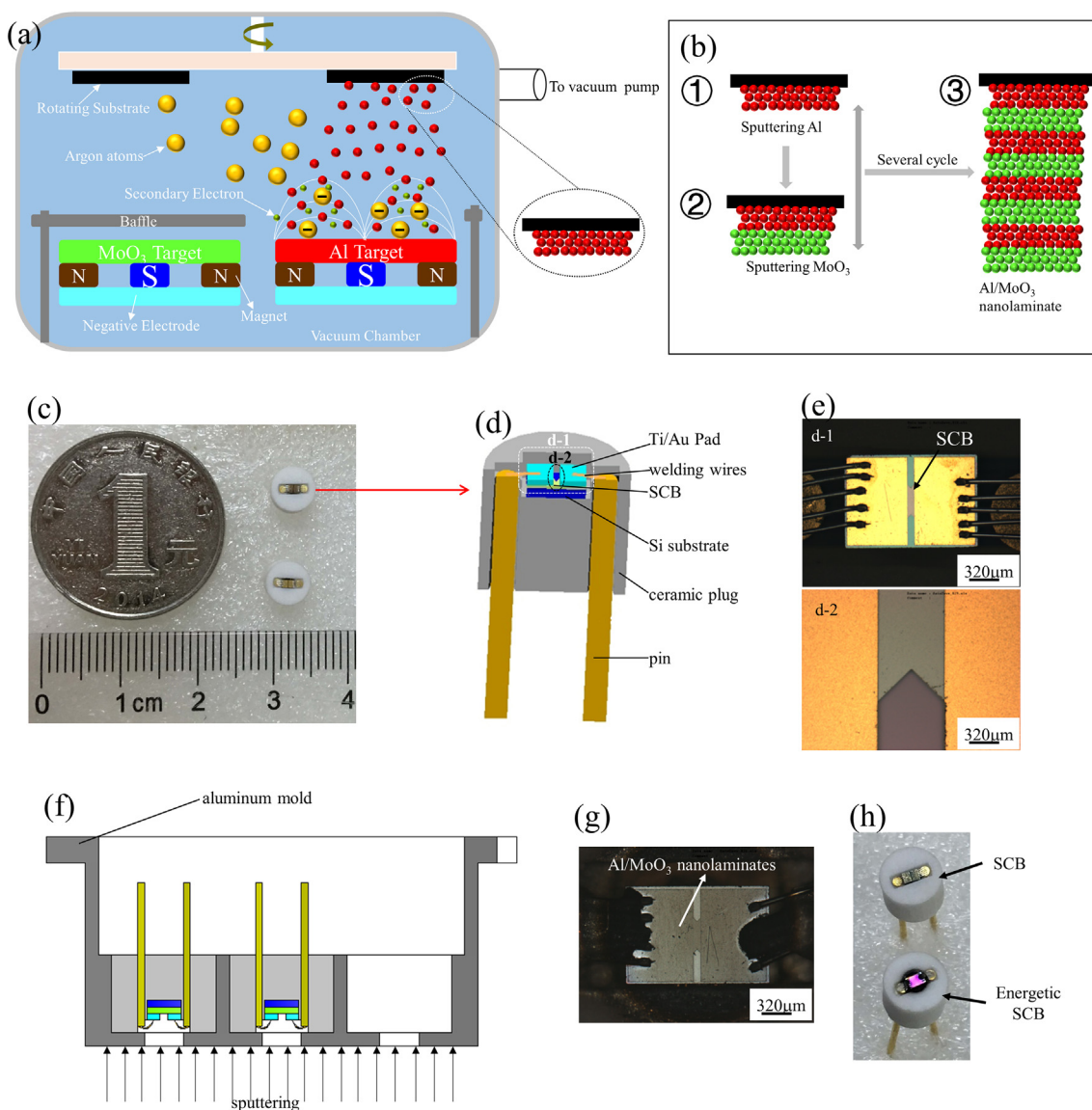


Fig. 1. Schematic of (a) magnetron sputtering system for depositing multilayer thin films, and (b) the fabrication process of Al/MoO₃ multilayer films; (c) photograph, (d) schematic structure and (e) optical microscope images of the SCB initiator, (f) the schematic of a mold for magnetron sputtering, (g) photograph and (h) top-view optical image of SCB after Al/MoO₃ nanolaminates deposition.

Table 1
Al/MoO₃ nanolaminates with different internal structure.

Equivalence ratio	Single Al/ nm	Single MoO ₃ /nm	Bilayer thickness/nm	Total thickness/ μ m
2	86	64	150	3
1	60	90	150	3
2/3	46	104	150	3

chemical characteristic of this energy storage materials play an important role in their performance of energy storage. As a typical energy storage material, energetic materials which contain oxidizer and fuel to store considerable chemical energy have been attracted much attention for their broad potential applications in both civilian and military fields [5–7]. However, energetic materials demonstrate low energy release rate and even unreacted when in micro energy storage device because of the long diffusion distance between fuels and oxidizers [8]. Therefore, it is highly important to develop novel energetic materials to improve the performance for this micro energy storage device.

With the development of nanotechnology, various teams have

introduced “nano” into energetic materials with new and special structures to enhance the reactivity of energetic materials, such as nano powder [9–12], core-shell structure [13–15], metal organic frameworks [16,17], macroporous structure [18,19], nanofilms [20,21]. Among these nano energetic materials, the nanolaminate with two-dimensional (2D) nanofilms systems have attracted great interest due to their unique mechanical, semiconductor, and electrical properties resulting from absolutely dense and ultra-fine grained structures [22,23]. The performance of deposited nanolaminate is determined by their compositions, arrangements and thicknesses. Periodically stacked multilayered films provide a fascinating structural element in implementing highly functional nanolaminate at molecular or sub-nanometer scale by increasing interfacial contact area and shorten diffusion distance among different layers [24,25]. In addition, these kind of nanolaminate can be easily integrated with microelectronic and mechanical systems (MEMS) [26–29], which provides potential applications in the field of miniature energy storage devices.

Based on the advantages listed above, energetic materials with nanolaminate structure possess high energy density in micro energy storage device as well as controllable reactivity performance through

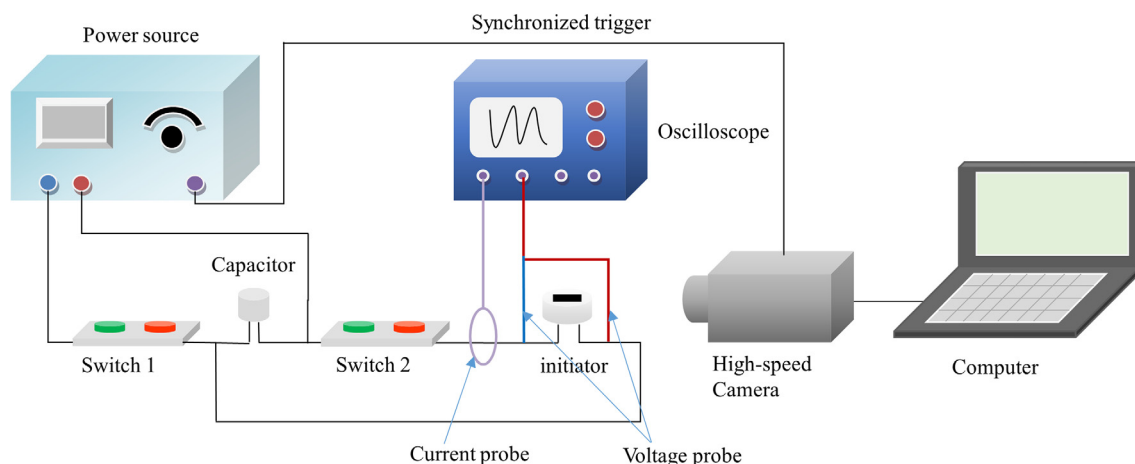


Fig. 2. Schematic of ignition test system for micro initiator. The voltage and current single was recorded by the oscilloscope, and ignition process was recorded synchronously using the high-speed camera.

thickness control of each layer and interfacial chemical reaction between layers in the synthesis process. Therefore, this could be produced for engineering applications and bring benefit of adjustable properties for micro energy storage devices.

In this study, energetic nanolaminate materials were designed and fabricated through magnetron sputtering method by periodically depositing oxidizer MoO_3 and fuel Al due to the high energy density (1124 cal/g, 4297 cal/cm³) and adiabatic flame temperature (3253 K) [30] in Al/ MoO_3 reaction. Three kinds of micro energy storage devices were fabricated by in situ depositing Al/ MoO_3 nanolaminates with different internal structure on a semiconductor bridge. The energy release process of these micro energy storage devices was investigated systematically under capacity discharge conditions. Furthermore, the reaction mechanism of the nanolaminates is also studied under argon and vacuum ignition.

2. Experimental

2.1. Al/ MoO_3 nanolaminates preparation

The Al/ MoO_3 nanolaminates were deposited on a silicon substrate by magnetron sputtering, as shown in Fig. 1a. The Al target disk ($\Phi 76 \text{ mm} \times 5 \text{ mm}$, purity > 99.999%) and MoO_3 target disk ($\Phi 76 \text{ mm} \times 5 \text{ mm}$, purity > 99.999%) were purchased from Zhongnuo Xincui Technology Corporation and used for depositing Al and MoO_3 films. The pressure in the vacuum chamber was pumped away below $9 \times 10^{-4} \text{ Pa}$ before deposition. Then, ultrahigh purity argon (99.99%) was passed into the chamber as the working gas with a flux of 16 sccm to keep the working pressure at 0.4 Pa. After this, multilayer films were fabricated by alternating Al and MoO_3 deposition periodically, as shown in Fig. 1b. To optimize film quality and remain stable velocity of deposition, the Al target was sputtered with direct-current (DC) magnetron at 150 W and MoO_3 target was sputtered with radio frequency (RF) magnetron at 200 W. The thickness of each individual layer could be controlled precisely by adjusting the sputtering time, which would be easily obtained the nanolaminate with different single thickness. The bilayer thickness of Al/ MoO_3 was kept at 150 nm, and the single layer Al and MoO_3 were 46 nm/104 nm, 60 nm/90 nm and 86 nm/64 nm, respectively, corresponding to the equivalence ratio from 2 to 2/3. The total thickness of nanolaminate was 3 μm , as shown in Table 1.

2.2. Fabrication of energetic micro initiator

Semiconductor bridge (SCB) sample was consisted of polysilicon membrane with special geometric shapes on the silicon substrate, which manufactured with a conventional complementary metal oxide

semiconductor (CMOS) technology to ensure production in batches and high level of integration [31]. Phosphorus atoms of high concentrations were doped on the polycrystalline silicon with a concentration of 10^{20} phosphorus atoms per cubic centimeter, and a thickness of 2 μm . The patterning of SCB with special bridge shape was realized by the plasma etching process. Fig. 1c shows a typical SCB initiator packaged with ceramic plug for ease of use. It consisted of SCB chip, two Ti/Au pads, welding wires, two pins and a ceramic plug (Fig. 1d). The SCB chip had a double V type with the angle of 90° and the size was 380 μm (width) \times 80 μm (length) \times 2 μm (thickness) (Fig. 1e). The total size of the packaged SCB initiator was 6 mm (diameter) \times 4 mm (height) (Fig. 1c). To deposit the nanolaminate on the SCB regions, an aluminum mold with specialized grooves was designed, as shown in Fig. 1f. Before the deposition of nanolaminate, SCB initiator was inserted into the top groove with the same diameter of initiator. Then, Al/ MoO_3 nanolaminates were in situ sputtered onto the SCB chip through the bottom groove with the diameter of 3 mm. The energetic initiator (micro energy storage energy device) was shown in Fig. 1g and h.

2.3. Materials characterization method

The morphology of the Al/ MoO_3 nanolaminate was analyzed using scanning electron microscopy (SEM, ZEISS, EVO 10) and its composition was determined with an energy dispersive spectroscopy (EDS, Bruker Quanta 200). The samples were peeled off and transferred in an alumina crucible for thermal analysis. The exothermic reaction in the various Al/ MoO_3 nanolaminates was characterized by using differential scanning calorimetry (DSC, NETZSCH STA 449C) with a temperature range from 30 °C to 800 °C at a heating rate of 20 °C/min under a high purity nitrogen flow of 20 mL/min.

2.4. Ignition test of micro initiator

A capacitor(47 μF) discharge firing circuit test system was performed to test electrical explosive characteristics of energetic SCB initiator, which is illustrated in Fig. 2a. It mainly consisted of a direct current power supply, two switch, a storage capacitor, a voltage probe, a current probe, a digital phosphor oscilloscope (LeCroy TM 44Xs) and a high speed camera (HG-100K, Redlake, USA) accompanied with a recorded computer. In the process of experiment, the sample was connected into the circuit by the two pins of energetic SCB initiator, and then switch 1 was turned on to charge the capacitor with the preset voltage. After the charging process was completed, switch 1 was turned off and switch 2 was closed. So the energetic SCB initiator was initiated by capacitor discharging. At the same time, the voltage and current single was recorded by the oscilloscope, and energy release process of

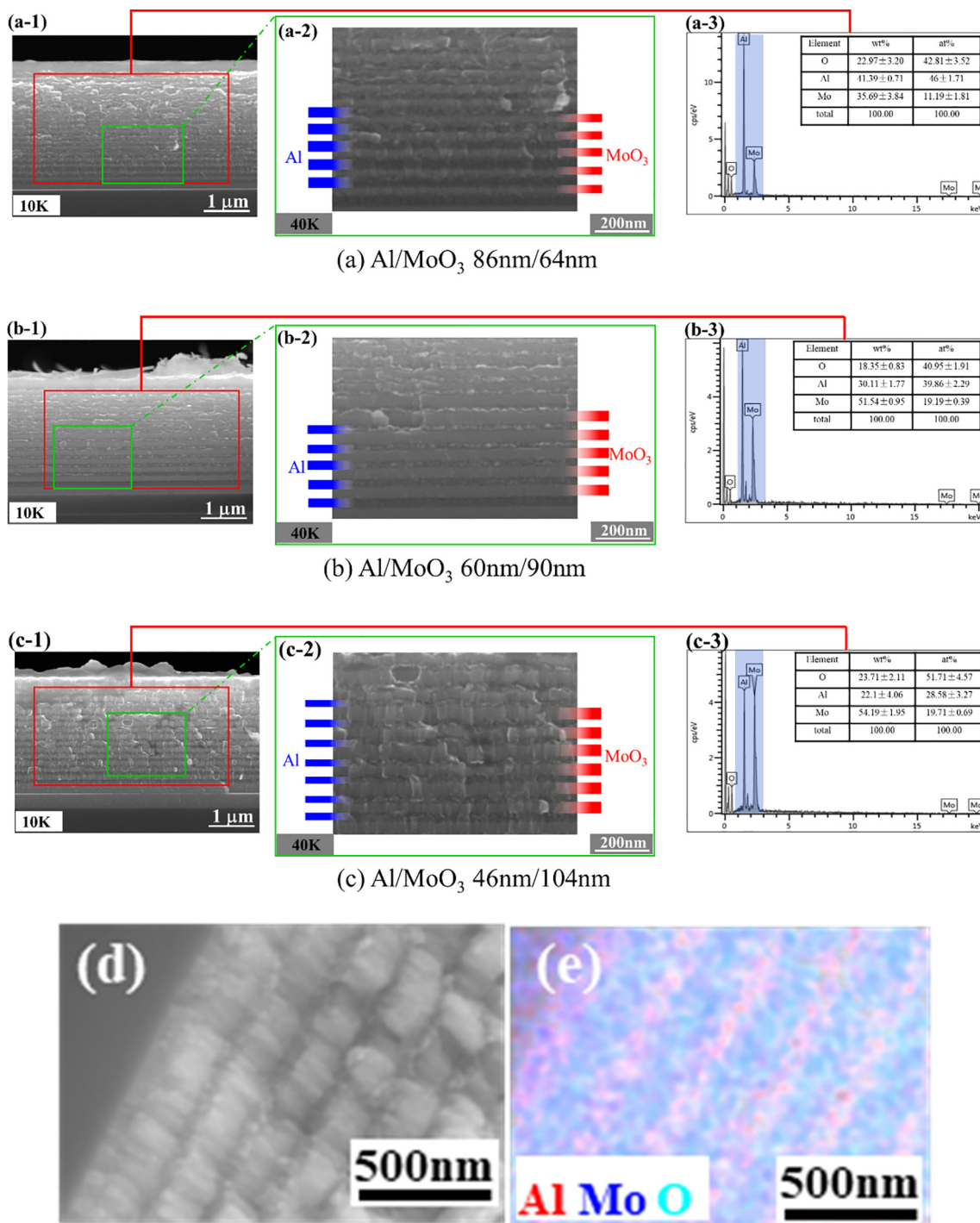


Fig. 3. Cross-sectional SEM image and EDS patterns of Al/MoO₃ nanolaminates. Al/MoO₃ nanolaminates (a) 86 nm/64 nm, (b) 60 nm/90 nm, (c) 46 nm/104 nm. (d) SEM and (e) EDS image of Al/MoO₃ nanolaminates (60 nm/90 nm).

these initiator was recorded synchronously using the high-speed camera (HG-100K) at 50,000 frames per second. Triple tests were performed with the charging voltage ranging from 30 to 50 V at 5 V increments, and then the results were averaged.

2.5. Ignition test of nanolaminate in argon and vacuum circumstance

A quick heating ignition experiment was used to do the ignition test under argon and vacuum circumstance. Firstly, Al/MoO₃ nanolaminate sample was deposited on a filament by magnetron sputtering. And then, the filament was put into a sealed chamber with argon (1 atm) or

vacuum (4.6×10^{-6} torr) circumstance. Finally, nearly 20V power supply was applied to the filament and the nanolaminate sample was ignited by joule heating. At the same time, a high-speed digital video imaging of the ignition process was recorded with a digital camera, at a frame rate of 67,000 frames per second and a resolution of 256 × 256.

3. Results and discussion

3.1. Morphology and thermodynamic properties of Al/MoO₃ nanolaminates

To understand the internal structure and composition of the Al/

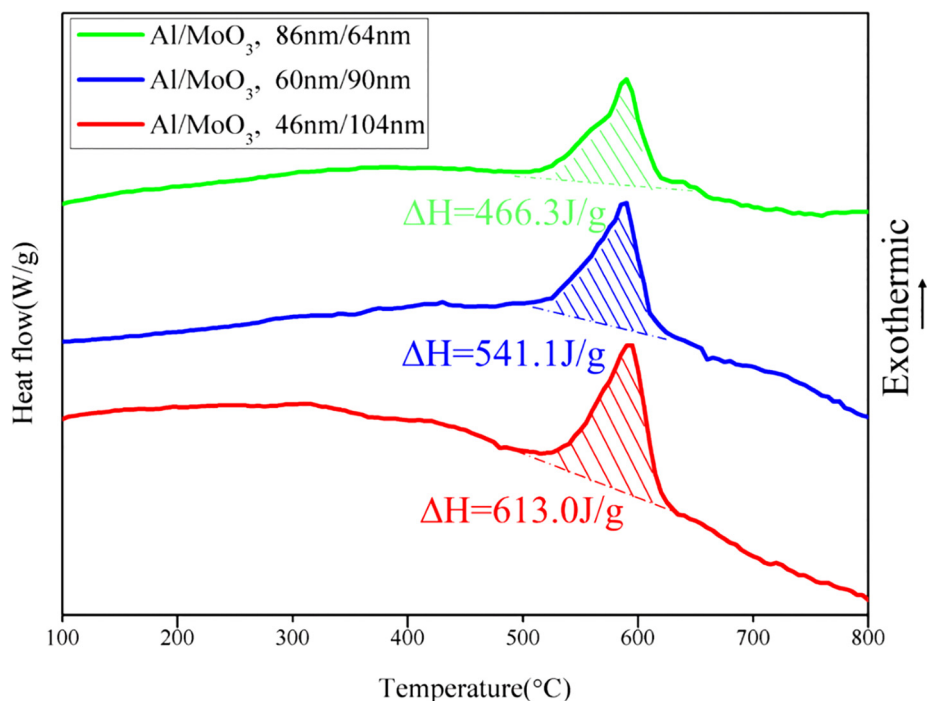


Fig. 4. DSC curves of three kinds of Al/MoO₃ nanolaminates at a heating rate of 20 °C/min in argon.

MoO₃ nanolaminates, SEM in cross-sectional view accompanied with EDS is applied to characterize the three kind of nanolaminates. The Al layer and MoO₃ layer contact closely and deposit periodicity as designed thickness. The obvious boundary can be distinguished between the two layers (Fig. 3a-1, 3b-1, 3c-1). More detailed structure of these three samples in the selected area (the green frame area in Fig. 3a-1, 3b-1, 3c-1) is shown in Fig. 3a-2, 3b-2 and 3c-2. The thickness of nanolaminate Al/MoO₃ 46 nm/104 nm in each bilayer is 46 nm (Al), 104 nm (MoO₃) respectively, thus a significant thickness difference can be seen between two layers from Fig. 3c-2. On the contrary, this situation is not such apparent in nanolaminate Al/MoO₃ 86 nm/64 nm with 86 nm Al and 64 nm MoO₃ in each bilayer (Fig. 3a-2). This result is consistent with our design listed in Table 1. The composition of these three nanolaminates in the selected red frame area in Fig. 3a-1, b-1 and c-1 is confirmed with Mo, O, Al (Fig. 3a-3, 3b-3 and 3c-3). Furthermore, the Mo content is more than Al in Fig. 3c-3 while it is less than Al in Fig. 3a-3 (as shown in the blue shadow area). EDS mapping in Fig. 3e confirms the ordered arrangement of Al, O, Mo element in the Al/MoO₃ nanolaminates. This result also demonstrates different internal structure design in these three nanolaminates, which make it possible for micro energy storage devices with adjust properties.

The exothermic reaction of these three energetic Al/MoO₃ nanolaminates is analyzed with Differential Scanning Calorimetry (DSC), and the results were shown in Fig. 4. The exothermic reaction of Al and MoO₃ occurs continuously in the range of 500–650 °C and the exothermic peak of these three energetic Al/MoO₃ nanolaminates seem to be consistent at 590 °C, which is below the melt point of Al. This reveals that the reaction of this three nanolaminates is solid-solid reaction, and the reaction sensitivity seems unchanged with the fixed bilayer thickness. Furthermore, the total heat release of these exothermic peak for these three nanolaminates is 466.3 J/g (Al/MoO₃ 86 nm/64 nm), 541.1 J/g (Al/MoO₃ 60 nm/90 nm), 613.0 J/g (Al/MoO₃ 46 nm/104 nm), respectively. Surprisingly, the maximum heat release among these three samples is not Al/MoO₃ 60 nm/90 nm at theoretical stoichiometric ratio but Al/MoO₃ 46 nm/104 nm. The reason maybe that oxygen exchange between Al and MoO₃ will increase with the increasing the content of oxidizing agent and the fuel maybe react more fully in rich oxidizer atmosphere as result in higher reactivity for this

kind of nanolaminate.

3.2. Energy release performances of energetic SCB initiator

The reaction dynamic processes of electric explosion for these energy storage devices were recorded simultaneously by high-speed camera all discharged at 50 V/47 μF, as shown in Fig. 5. The interval between adjoining pictures is 20 μs, and the specific flame structures in different electric explosion stages have been observed. The flame area is also calculated to make a quantitative evaluation of ignition performance for these initiators. Using digital image processing techniques measurement, the electric explosion process digital image banalization operation was processed and then the pixel with bright area in this image was calculate it by matlab [32]. A small bright flash of purple is observed at the 20 μs for all initiators after triggering, which is regard as plasma generated by the electric explosion of SCB. And the flame duration time of SCB is about 100 μs, and the maximum flame area is measured as 9.56 mm². While for energetic SCB initiators, except for the plasma, a fierce combustion process with larger quantities of ejected product particles is also observed because of the reaction of Al/MoO₃ nanolaminate, which significantly extend the flame duration time and enhance the intensity of flame. The reaction reactivity varies with the arrangement of Al and MoO₃. The flame duration time and maximum flame area of energetic SCB 46 nm/104 nm are measured at 600 μs and 20.40 mm², which is longer than that of energetic SCB 60 nm/90 nm at theoretical stoichiometric ratio with 440 μs and 15.10 mm². In addition, the ignition process only lasts 140 μs for energetic SCB 86 nm/64 nm. This result is in good agreement with the DSC result revealing Al/MoO₃ 46 nm/104 nm releases largest heat energy among three nanolaminates, which demonstrates the energy release ability of these energy storage device can be controlled with different internal structure of nanolaminates.

The initiator device after ignition was shown in the right side frames of Fig. 5. For SCB, the central region of bridge is exploded by the electric energy. As for energetic SCB, the reaction region of nanolaminate is also observed and the images clearly indicates that the reaction zones of the nanolaminate increases with increase of MoO₃ content discharged with 50 V/47 μF. This results also consistent with high speed

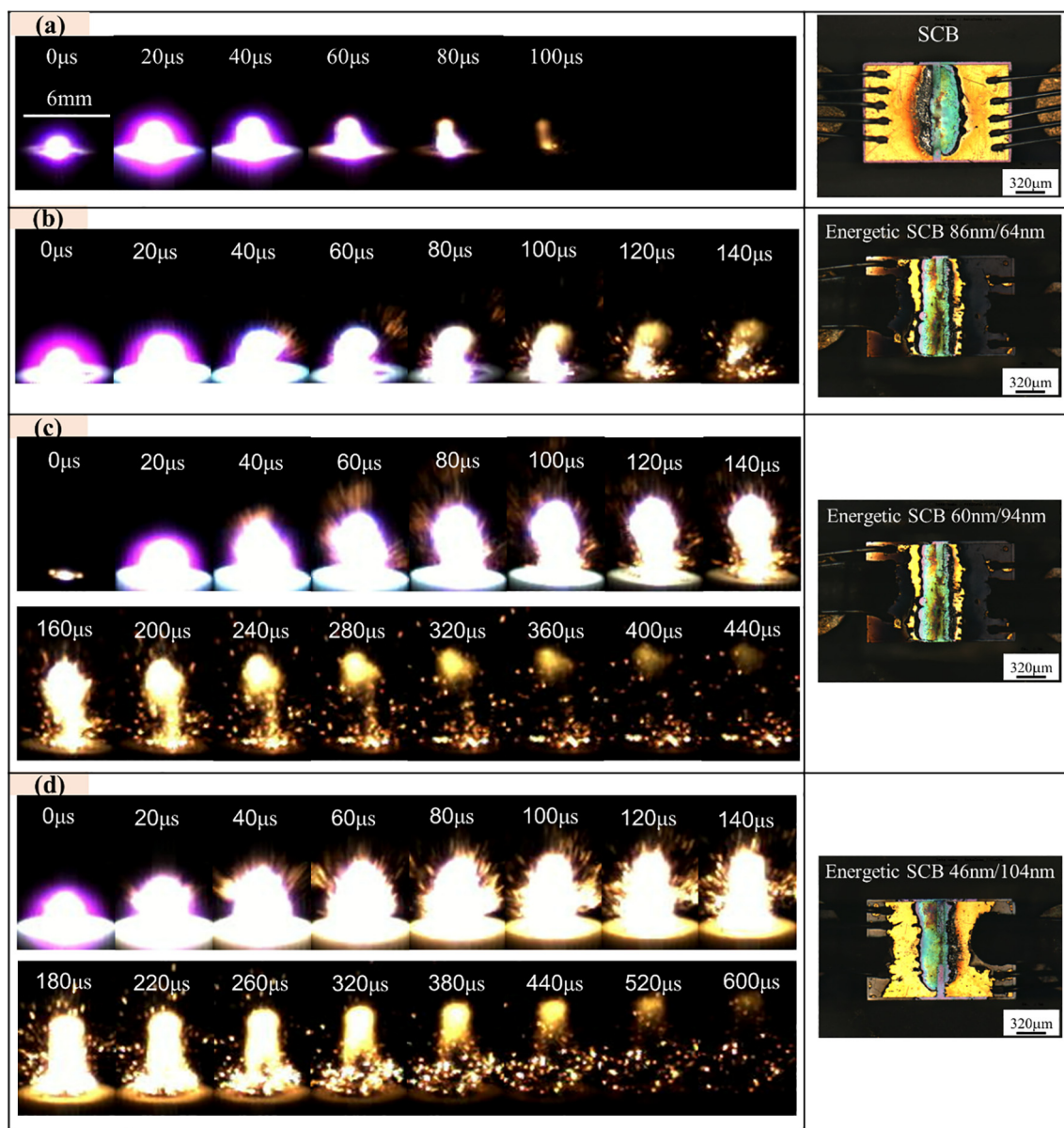


Fig. 5. High-speed images of electric process for various initiators at 50 V/47 μF and its optical microscope images after ignition, (a) SCB; (b) Energetic SCB 86 nm/64 nm; (c) Energetic SCB 60 nm/90 nm, (d) Energetic SCB 46 nm/104 nm.

recording displaying largest flame duration time and maximum flame area for energetic SCB 46 nm/104 nm. When compared with our previous work [33], the reactivity of nanolaminate can also be enhanced to reduce the single layer Al and MoO_3 . The Al/ MoO_3 nanolaminate can completely react when the bilayer thickness was 50 nm. It seems that the influence of bilayer thickness on the reactivity of Al/ MoO_3 nanolaminate is greater than that of the species ratio.

The electrical explosion process of energetic SCB initiator involves the outbreak of SCB and the chemical combustion of nanolaminate. The typical voltage-current-resistance (VCR) curves of these initiators under 40 V/47 μF were shown in Fig. 6. Some typical terminal points were defined with the variation of voltage curves. The voltage increased from t_0 to its first peak t_1 . After this, the voltage decreased to t_2 and then increased to its second peak t_3 . Finally, the SCB would break and the current would downward to zero at t_4 . The SCB experiences warming ($t_0 \rightarrow t_1$), melting ($t_1 \rightarrow t_2$), gasification ($t_2 \rightarrow t_3$), outbreak ($t_3 \rightarrow t_4$) and the characteristic parameters are defined according to the VCR curves [34]. It is clearly that the VCR curve in energetic SCB is similar to SCB, which involves four process. The difference is that the VCR curve in

energetic SCB has a stagnation in the process $t_0 \rightarrow t_1$ when compared with SCB. The second voltage peak is a signal the emergence of plasma where the bridge material was entirely gasification [35]. Therefore, this point is also called critical burst point (t_c). t_c is an important parameter for assessing the energy release performance of energetic SCB initiator. Fig. 7 summarized critical burst time for these initiators at different discharge voltages. The result shows that SCB demonstrates lowest t_c under the same voltage. And the t_c in energetic SCB 86 nm/64 nm decreases sharply following the discharge voltage from 16 μs to 7 μs , while this downward trend is not much strong in energetic SCB 46 nm/104 nm from 8 μs to 5 μs . This is because the nanolaminate may absorb heat from SCB, which increase the outbreak time compared with SCB. Moreover, MoO_3 (9.310 W/m/K) has lower thermal conductivity than Al (240 W/m/K [36]) as a result of lower heat loss and shorter t_c for energetic SCB 46 nm/104 nm. In addition, the difference of t_c among these initiators is obvious at low voltage, while it seems to be consistent under 50 V. Because the process of melting and gasification in SCB is expedited under high discharge voltage, which shortens the lag of t_c .

Fig. 7b summarizes the flame duration of various initiators under

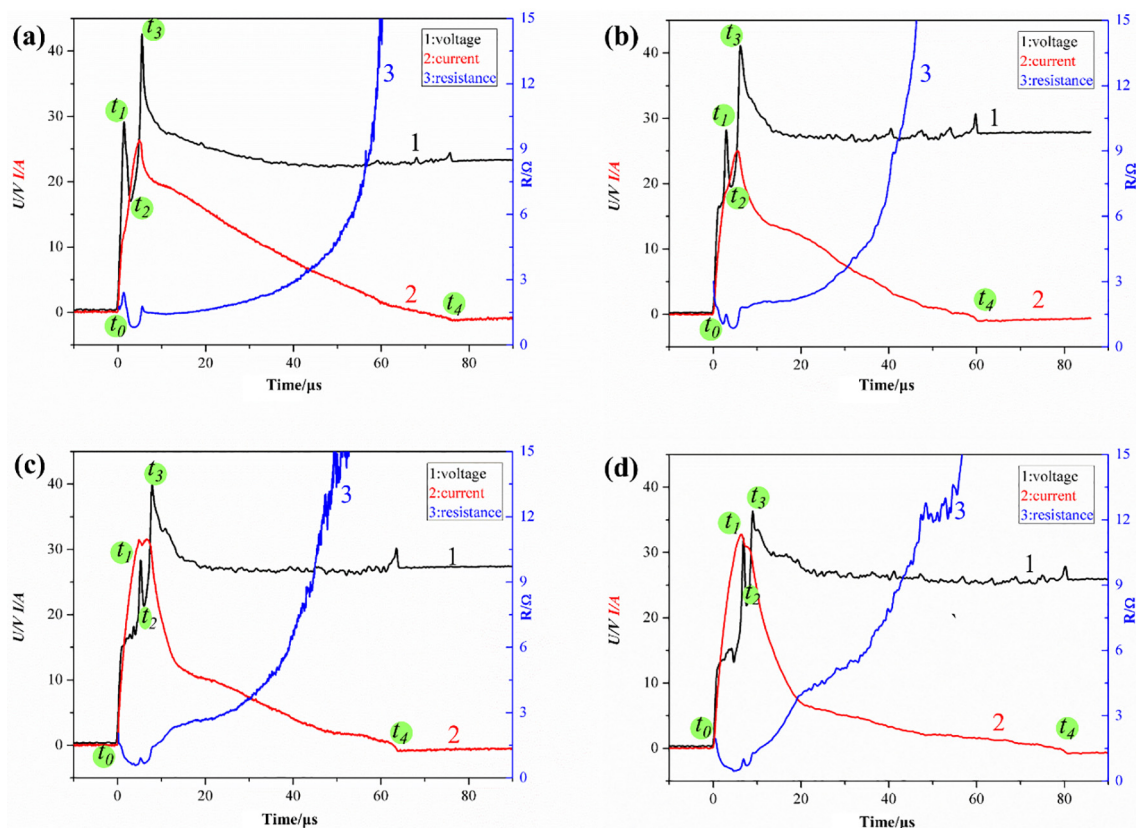


Fig. 6. Curves of current, voltage, and resistance varied with time for all initiators discharged with 40 V/47μF, (a) SCB; (b) Energetic SCB 46 nm/104 nm; (c) Energetic SCB 60 nm/90 nm, (d) Energetic SCB 86 nm/64 nm.

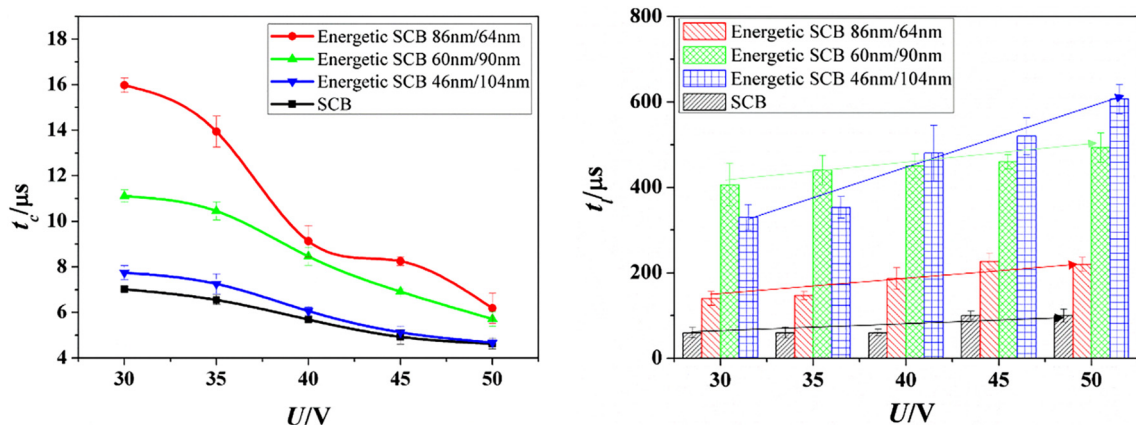


Fig. 7. (a) Critical burst time and (b) ignition duration for various initiator at different discharge voltages. (here, t_c is the critical burst time and t_i is ignition duration).

different discharge voltage. Without nanolaminate, t_i only reaches about nearly 100 μs, while t_i can be greatly enhanced for energetic SCB. The t_i is positively proportional to the discharged voltage for three energetic SCB. Energetic SCB 46 nm/104 nm has a fastest growing t_i from 300 μs to 600 μs, which is 6 times that of the original SCB. Then is the energetic SCB 86 nm/64 nm from 150 μs to 200 μs. And it seems to be stable at 400 μs for energetic SCB 60 nm/90 nm. The energetic SCB 46 nm/104 nm is sensitive to external stimuli when compared with energetic SCB 60 nm/90 nm. The oxygen diffusion between Al/MoO₃ is not such fierce under low external stimuli, while it is far more fierce under high external stimuli. Therefore, the t_i in energetic SCB 60 nm/90 nm at 30 V and 35 V are higher than that of energetic SCB 46 nm/104 nm. As the result, reaction of this system can be controlled by designing the internal structure of the Al/MoO₃ nanolaminates. Hence,

there is much prospect of the application of Al/MoO₃ nanolaminate energetic material on microigniter device to implement special function.

3.3. Probing the reaction mechanism of Al/MoO₃ nanolaminates

On the basis of the above results, the internal structure of Al/MoO₃ has a direct impact on its reactivity, which realized controlled energy release performance of micro initiator. The DSC and ignition test both show that Al/MoO₃ with oxide agent rich demonstrate greater performance. There is a doubt that the ignition test is conducted in the open air, where the oxygen may react with Al/MoO₃ nanolaminates. Thus Al/MoO₃ with fuel rich is supposed to behave higher reactivity. However, the ignition test reveals the opposite result. It seems that the

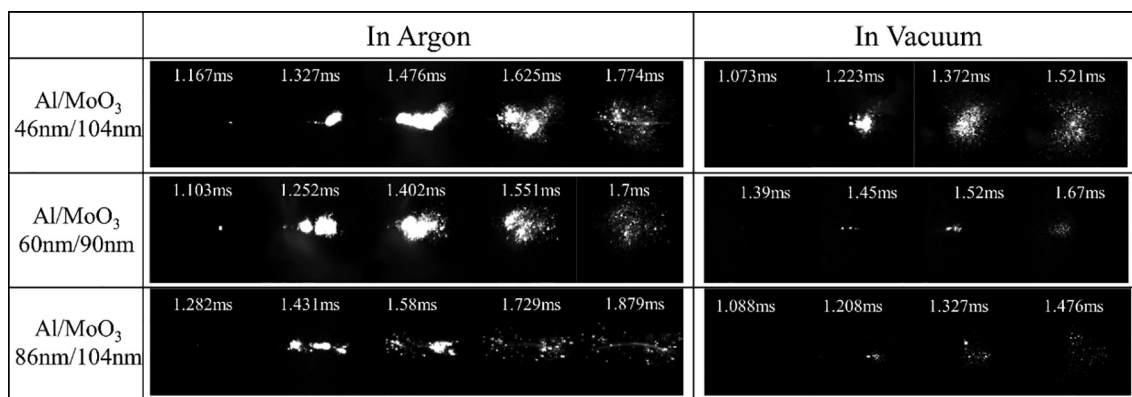


Fig. 8. Frames from the high speed video of three samples in argon and vacuum atmosphere.

Table 2

Summary of the expected behavior of oxidizers under heating [37–39]. (here, *s* is solid phase of products, *l* is liquid phase of products, *g* is gas phase of products).

Oxidizer	Temperature (K)	Event	Products	Temperature (K)	Event	Main Products
CuO	~800	decomposes	CuO (<i>s</i>), O ₂ (<i>g</i>)	1150	decomposes	Cu (<i>s</i>), O ₂ (<i>g</i>)
Fe ₂ O ₃	~1100	decomposes	Fe ₃ O ₄ (<i>s</i>), O ₂ (<i>g</i>)	1500	decomposes	Fe (<i>s</i>), O ₂ (<i>g</i>)
MoO ₃	1075	melts	MoO ₃ (<i>l</i>)	1428	boils	MoO ₃ (<i>g</i>)

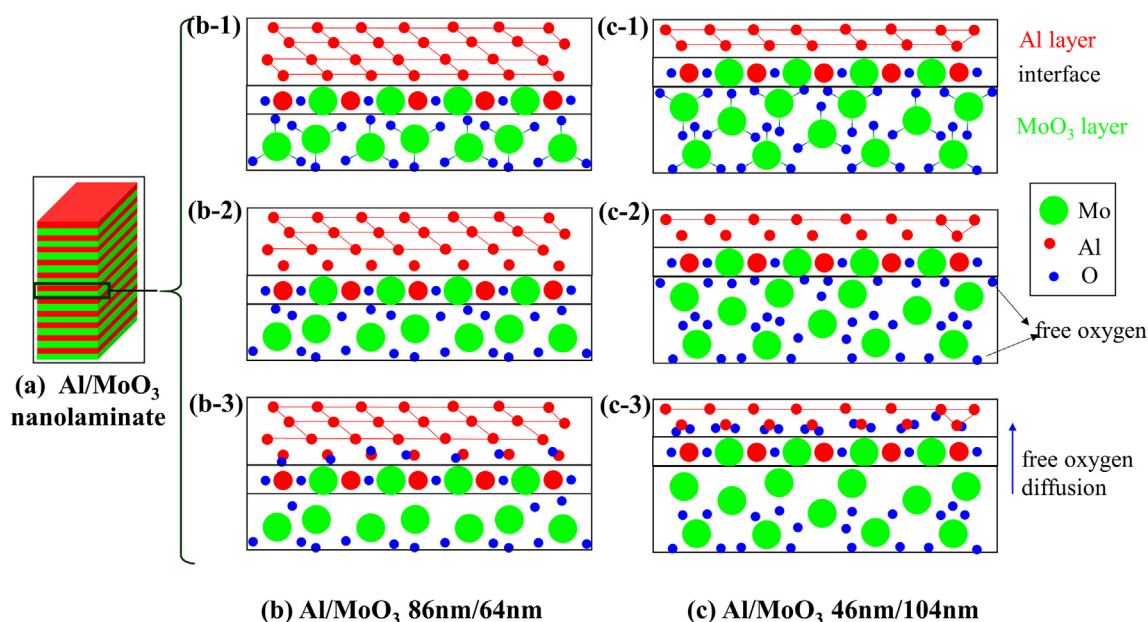


Fig. 9. (a) Schematic of Al/MoO₃ nanolaminate, (b) the oxygen diffusion process of Al/MoO₃ 86 nm/64 nm and (c) the oxygen diffusion process of Al/MoO₃ 46 nm/104 nm.

oxide agent and reducing agent only react itself since the closely contact between the two species. And the oxide agent seems play an important role on the energetic prosperity of this kind of nanolaminate. In order to investigate the influence of the outer oxide and inner oxide on the energetic performance of Al/MoO₃ nanolaminate, Al/MoO₃ nanolaminate coated filament was placed into argon and vacuum atmosphere and then ignited by joule heating. Fig. 8 in the left section shows some frames taken from the high-speed video of experiments performed on three Al/MoO₃ nanolaminate in argon (1 atm) atmosphere. As can be seen, the Al/MoO₃ 86 nm/64 nm only reacted very weakly. Comparatively, both the Al/MoO₃ 60 nm/90 nm and Al/MoO₃ 46 nm/104 nm reacted far more violently. This phenomenon is very similar to the ignition test in the open air. It suggests that the outer oxide is hard to react with Al in this kind of multilayered films, as Al/MoO₃ nanolaminates have high energy releasing rate and Al films is intimately

contacted with MoO₃ film.

Interestingly, a violent brightness for Al/MoO₃ 46 nm/104 nm under vacuum circumstance also can be investigated from the right frame of Fig. 8. However, a weaker reaction is observed for Al/MoO₃ 60 nm/90 nm and Al/MoO₃ 46 nm/104 nm under the same condition. For nano Al/metal oxide reaction, two kinds of reaction mechanism are summarized with relevant researcher [37]. The first one is condensed state reaction process (equation1), which the direct interfacial contact between fuel and oxidizer, leading to condensed state mobility of reactive species. The second one is gas state reaction process (Eq. (2)), which oxidizer firstly produces O₂ gas and then react with Al. Since the more MoO₃ in Al/MoO₃ nanolaminate, the more violent reaction happened under vacuum circumstance, it is clearly that Al/MoO₃ nanolaminate is condensed state reaction process. If the reaction produces any O₂ gas, gas will be spread rapidly. Another reason is that MoO₃ didn't

release any gas calculated using the NASA-CEA software [38,39] when taking into account some of the thermodynamically predicted phase changes or decompositions, as shown in Table 2. Unlike CuO and Fe₂O₃, which would decompose into respective sub-oxides Cu₂O (s) and Fe₃O₄ (s), releasing O₂ [40], before decomposing to the zero-valent metal at higher temperatures, MoO₃ melts first into the liquid phase at 1075 K and then boils at 1428 K. Hence, oxygen transport in condensed phases may be driving in Al/MoO₃ nanolaminate. In addition, a one-dimension diffusion model was established in our previous work when increasing the interfacial number between Al and MoO₃ [33], and reducing the mass transfer distance of oxidizer and fuel, which further verify the diffusion reaction mechanism.



Based on the results of previous work and our findings in this study, the reaction mechanism for Al/MoO₃ nanolaminate can be summarized in Fig. 9. For the Al/MoO₃ nanolaminate, the reaction starts in the interface as the atomic exchange across the interfacial layer. Free oxygen in nanolaminate maybe be generated from the reduction of MoO₃ when triggered by outer stimulation (Fig. 9b-2 and 9c-2). Thus, the free oxygen may diffuse into Al layer across the interfacial layer and oxide the Al (Fig. 9b-3 and 9c-3). Because of the high MoO₃ concentration in Al/MoO₃ 46 nm/104 nm, more O atom will diffuse into the fuel layer (Fig. 9c-3) and accelerate the oxidation process of Al. In addition, since the thinner Al layer in Al/MoO₃ 46 nm/104 nm among three kinds of nanolaminates, the oxidization of Al is more likely to occur. So the transport of oxidizer species can increase the reaction rate and thus enhances the reactivity. Thus the reactive properties of this multilayered laminated structure materials can be enhanced with the incorporation of high oxygen concentration, in some cases.

4. Conclusion

In summary, energetic Al/MoO₃ nanolaminates with different ratios were designed and prepared to realize controllable ability of micro energy store device. Three kinds of energetic Al/MoO₃ nanolaminates (Al/MoO₃ 86 nm/64 nm, Al/MoO₃ 60 nm/90 nm, Al/MoO₃ 46 nm/104 nm) were fabricated by magnetron sputtering, and the structure and chemical composition were confirmed by SEM and EDS. The periodic multilayer structure could be clearly visible, which was composed of stacked Al layers and MoO₃ layers with various thickness. DSC showed that the main exothermic reaction of Al and MoO₃ occurred continuously in the range of 500–650 °C and the exothermic peak of these three energetic Al/MoO₃ nanolaminate seemed to be consistent at 590 °C. The total heat release of these exothermic peak for these three nanolaminate were 466.3 J/g (Al/MoO₃ 86 nm/64 nm), 541.1 J/g (Al/MoO₃ 60 nm/90 nm) and 613.0 J/g (Al/MoO₃ 46 nm/104 nm), respectively. The micro energy store devices (energetic SCB 86 nm/64 nm, energetic SCB 60 nm/90 nm, energetic SCB 46 nm/104 nm) were in situ integrated on SCB based on our Al/MoO₃ nanolaminates, which would be successfully ignited with electric stimulus. The ignition duration of the energetic SCB 86 nm/64 nm, energetic SCB 60 nm/90 nm, energetic SCB 46 nm/104 nm were recorded at 140, 440, 600 μs, respectively, both discharged at 47μF/50 V. Energetic SCB 46 nm/104 nm exhibits excellent performances with a short burst time, highest flame duration time and maximum flame area. Analysis of the reaction mechanism indicated that Al/MoO₃ nanolaminate is a condensed state reaction process and the oxygen transportation in condensed phases may be a significant factor in the initiation of Al/MoO₃ multilayered films reaction, which suggested that reactive properties of this multilayered laminated structure materials could be improved with the increase of oxidizer concentration.

Acknowledgments

This work was supported by the Innovation Foundation of CASC (No. CASC150701), and the Outstanding Thesis Funds for Ph.D. Students of Nanjing University of Science and Technology. Jianbing Xu is grateful for the financial support from China Scholarship Council.

References

- [1] A.S. Arico, P. Bruce, B. Scrosati, J.-M. Tarascon, W. Van Schalkwijk, Nanostructured materials for advanced energy conversion and storage devices, *Materials For Sustainable Energy: A Collection of Peer-Reviewed Research and Review Articles* from Nature Publishing Group, World Scientific, 2011, pp. 148–159.
- [2] Y.G. Guo, J.S. Hu, L.J. Wan, Nanostructured materials for electrochemical energy conversion and storage devices, *Adv. Mater.* 20 (2008) 2878–2887.
- [3] C. Liu, F. Li, L.P. Ma, H.M. Cheng, Advanced materials for energy storage, *Adv. Mater.* 22 (2010) E28–E62.
- [4] L.F. Cabeza, A. Castell, C.D. Barreneche, A. De Gracia, A. Fernández, Materials used as PCM in thermal energy storage in buildings: a review, *Renewable Sustainable Energy Rev.* (2011) 151675–151695.
- [5] P.F. Pagoria, G.S. Lee, A.R. Mitchell, R.D. Schmidt, A review of energetic materials synthesis, *Thermochim. Acta* 384 (2002) 187–204.
- [6] D.M. Badgujar, M.B. Talawar, S.N. Asthana, P.P. Mahuliker, Advances in science and technology of modern energetic materials: an overview, *J. Hazard. Mater.* 151 (2008) 289–305.
- [7] D.G. Piercey, T.M. Klapoetke, Nanoscale aluminum-metal oxide (thermite) reactions for application in energetic materials, *Cent. Eur. J. Energetic Mater.* 7 (2010) 115–129.
- [8] C. Rossi, B. Larangot, D. Lagrange, A. Chaalane, Final characterizations of MEMS-based pyrotechnical microthrusters, *Sensors Actuat. A-Phys.* 121 (2005) 508–514.
- [9] H. Wang, G. Jian, G.C. Egan, M.R. Zachariah, Assembly and reactive properties of Al/CuO based nanothermite microparticles, *Combust. Flame* 161 (2014) 2203–2208.
- [10] Y. Jiang, S. Deng, S. Hong, J. Zhao, S. Huang, C.-C. Wu, J.L. Gottfried, K.-I. Nomura, Y. Li, S. Tiwari, R.K. Kalia, P. Vashishta, A. Nakano, X. Zheng, Energetic performance of optically activated aluminum/graphene oxide composites, *ACS Nano* (2018).
- [11] J. Guoqiang, L. Lu, R. Zachariah Michael, Facile Aerosol Route to Hollow CuO Spheres and its Superior Performance as an Oxidizer in Nanoenergetic Gas Generators, *Adv. Funct. Mater.* 23 (2013) 1341–1346.
- [12] J. Dai, J. Xu, F. Wang, Y. Tai, Y. Shen, R. Shen, Y. Ye, Facile formation of nitrocellulose-coated Al/Bi₂O₃ nanothermites with excellent energy output and improved electrostatic discharge safety, *Mater. Des.* 143 (2018) 93–103.
- [13] X. Zhou, D. Xu, G. Yang, Q. Zhang, J. Shen, J. Lu, K. Zhang, highly exothermic and superhydrophobic Mg/fluorocarbon core/shell nanoenergetic arrays, *ACS Appl. Mater. Interfaces* 6 (2014) 10497–10505.
- [14] X. Zhou, D.G. Xu, Q.B. Zhang, J. Lu, K.L. Zhang, Facile green In Situ Synthesis of Mg/CuO Core/Shell nanoenergetic arrays with a superior heat-release property and long-term storage stability, *ACS Appl. Mater. Interfaces* 5 (2013) 7641–7646.
- [15] X. Ke, X. Zhou, H. Gao, G. Hao, L. Xiao, T. Chen, J. Liu, W. Jiang, Surface functionalized core/shell structured CuO/Al nanothermite with long-term storage stability and steady combustion performance, *Mater. Des.* 140 (2018) 179–187.
- [16] J. Wang, W. Zhang, L. Wang, R. Shen, X. Xu, J. Ye, Y. Chao, Novel approach to the preparation of organic energetic film for microelectromechanical systems and microactuator applications, *ACS Appl. Mater. Interfaces* 6 (2014) 10992–10996.
- [17] W. Qianyou, F. Xiao, W. Shan, S. Naimeng, C. Yifa, T. Wenchao, H. Yuzhen, Y. Li, W. Bo, Metal-organic framework templated synthesis of copper azide as the primary explosive with low electrostatic sensitivity and excellent initiation ability, *Adv. Mater.* 28 (2016) 5837–5843.
- [18] C.P. Yu, W.C. Zhang, R.Q. Shen, X. Xu, J. Cheng, J.H. Ye, Z.C. Qin, Y.M. Chao, 3D ordered macroporous NiO/Al nanothermite film with significantly improved higher heat output, lower ignition temperature and less gas production, *Mater. Des.* 110 (2016) 304–310.
- [19] Y. Shen, J. Xu, N. Li, J. Dai, C. Ru, Y. Ye, R. Shen, W. Zhang, A micro-initiator realized by in-situ synthesis of three-dimensional porous copper azide and its ignition performance, *Chem. Eng. J.* 326 (2017) 1116–1124.
- [20] N.A. Manesh, S. Basu, R. Kumar, Experimental flame speed in multi-layered nanoenergetic materials, *Combust. Flame* 157 (2010) 476–480.
- [21] Y. Zhang, Y. Wang, M. Ai, H. Jiang, Y. Yan, X. Zhao, L. Wang, W. Zhang, Y. Li, Reactive B/Ti nano-multilayers with superior performance in plasma generation, *ACS Appl. Mater. Interfaces* 10 (2018) 21582–21589.
- [22] J. Azadmanjiri, C.C. Berndt, J. Wang, A. Kapoor, V.K. Srivastava, Nanolaminated composite materials: structure, interface role and applications, *RSC Adv.* 6 (2016) 109361–109385.
- [23] L.H. Kim, K. Kim, S. Park, Y.J. Jeong, H. Kim, D.S. Chung, S.H. Kim, C.E. Park, Al₂O₃/TiO₂ nanolaminate thin film encapsulation for organic thin film transistors via plasma-enhanced atomic layer deposition, *ACS Appl. Mater. Interfaces* 6 (2014) 6731–6738.
- [24] G.C. Egan, E.J. Mily, J.P. Maria, M.R. Zachariah, Probing the reaction dynamics of thermite nanolaminates, *J. Phys. Chem. C* 119 (2015) 20401–20408.
- [25] M. Bahrami, G. Taton, V. Conedera, L. Salvagnac, C. Tenaillon, P. Alphonse, C. Rossi, Magnetron sputtered Al-CuO nanolaminates: effect of stoichiometry and layers thickness on energy release and burning rate, *Propellants Explos. Pyrotech.*

- 39 (2014) 365–373.
- [26] X. Zhou, M. Torabi, J. Lu, R. Shen, K. Zhang, Nanostructured energetic composites: synthesis, ignition/combustion modeling, and applications, *ACS Appl. Mater. Interfaces* 6 (2014) 3058–3074.
- [27] G. Taton, D. Lagrange, V. Conedera, L. Renaud, C. Rossi, Micro-chip initiator realized by integrating Al/CuO multilayer nanothermite on polymeric membrane, *J. Micromech. Microeng.* 23 (2013) 105009.
- [28] J. Wang, X. Jiang, L. Zhang, Z. Qiao, B. Gao, G. Yang, H. Huang, Design and fabrication of energetic superlattice like-PTFE/Al with superior performance and application in functional micro-initiator, *Nano Energy* 12 (2015) 597–605.
- [29] J. Xu, Y. Tai, C. Ru, J. Dai, Y. Shen, Y. Ye, R. Shen, S. Fu, Characteristic of energetic semiconductor bridge based on Al/MoO_x energetic multilayer nanofilms with different modulation periods, *J. Appl. Phys.* 121 (2017) 113301.
- [30] S.H. Fischer, M. Grubelich, Theoretical energy release of thermites, intermetallics, and combustible metals, Sandia National Labs, Albuquerque, NM (US), 1998.
- [31] D.A. Benson, M.E. Larsen, A.M. Renlund, W.M. Trott, R.W. Bickes Jr., Semiconductor bridge: a plasma generator for the ignition of explosives, *J. Appl. Phys.* 62 (1987) 1622–1632.
- [32] C.M. Sabliov, D. Boldor, K.M. Keener, B.E. Farkas, Image processing method to determine surface area and volume of axi-symmetric agricultural products, *Int. J. Food Prop.* 5 (2002) 641–653.
- [33] J. Xu, Y. Tai, C. Ru, J. Dai, Y. Ye, R. Shen, P. Zhu, Tuning the ignition performance of a microchip initiator by integrating various Al/MoO₃ reactive multilayer films on a semiconductor bridge, *ACS Appl. Mater. Interfaces* 9 (2017) 5580–5589.
- [34] P. Zhu, J.S. Jiao, R.Q. Shen, Y.H. Ye, S. Fu, D.L. Li, Energetic semiconductor bridge device incorporating Al/MoO_x multilayer nanofilms and negative temperature coefficient thermistor chip, *J. Appl. Phys.* 115 (2014) 194502.
- [35] K.N. Lee, M.I. Park, S.H. Choi, C.O. Park, H.S. Uhm, Characteristics of plasma generated by polysilicon semiconductor bridge (SCB), *Sens. Actuators A-Phys.* 96 (2002) 252–257.
- [36] T. Yu, J. Xu, F. Wang, J. Dai, W. Zhang, Y. Ye, R. Shen, Experimental and modeling investigation on the self-propagating combustion behavior of Al-MoO₃ reactive multilayer films, *J. Appl. Phys.* 123 (2018) 235302.
- [37] G. Jian, S. Chowdhury, K. Sullivan, M.R. Zachariah, Nanothermite reactions: Is gas phase oxygen generation from the oxygen carrier an essential prerequisite to ignition? *Combust. Flame* 160 (2013) 432–437.
- [38] S. Gordon, B.J. McBride, Computer program for calculation of complex chemical equilibrium compositions and applications. Part 1, Analysis (1994).
- [39] W.M. Haynes, *CRC handbook of chemistry and physics*, CRC press 2014.
- [40] L. Zhou, N. Piekielek, S. Chowdhury, M.R. Zachariah, Time-resolved mass spectrometry of the exothermic reaction between nanoaluminum and metal oxides: the role of oxygen release, *J. Phys. Chem. C* 114 (2010) 14269–14275.